Journal of Organometallic Chemistry 694 (2009) 3012–3018

Contents lists available at ScienceDirect

Journal of Organometallic Chemistry

journal homepage: www.elsevier.com/locate/jorganchem

Theoretical investigation of electronic structures and excitation energies of hexaphyrin and its group 11 transition metal (III) complexes

Yu-Lan Zhu [a,*], Shu-Yu Zhou [b,c], Yu-He Kan [a,*], Zhong-Min Su [c]

[a] Department of Chemistry, Huaiyin Teachers College, Jiangsu Province Key Laboratory for Chemistry of Low-dimensional Materials, No. 111, Changjiang West Road, Huaian, Jiangsu 223300, PR China
[b] Department of Chemistry, College of Science, Yanbian University, Yanji 133002, PR China
[c] Institute of Functional Material Chemistry, Northeast Normal University, Changchun 130024, PR China

ARTICLE INFO

Article history:
Received 25 February 2009
Received in revised form 2 May 2009
Accepted 4 May 2009
Available online 8 May 2009

Keywords:
Hexaphyrin
Electronic structure
Electronic spectra
Time-dependent density functional theory
Spin–orbit coupling

ABSTRACT

Density functional theory is carried out to study hexaphyrin and its bis-metal and mixed bis-metal (M = Cu^{3+}, Ag^{3+}, and Au^{3+}) complexes. The electronic structures and bonding situations of them are studied by using natural bond orbital approach and the topological analysis of the electron localization function. Electronic spectra are investigated by using time-dependent density functional theory. The introduction of group 11 transition metals leads to red shifts in the spectra of these metal complexes with respect to that of hexaphyrin. Moreover, it is noteworthy that the spectra of copper contained complexes are mainly derived from combination of ligand-to-metal charge transfer and ligand-to-ligand charge transfer transitions. In addition, the relativistic time-dependent density functional theory with spin–orbit coupling calculations indicate that the effects of spin–orbit coupling on the excitation energies are so small that it is safe enough to neglect spin–orbit coupling for these systems.

1. Introduction

In recent years, considerable advancements have been made in expanded porphyrins that possess attractive photophysical, electronic and coordination properties which cannot be realized in normal porphyrin systems [1–8]. Expanded porphyrins including more than four pyrrole rings have been demonstrated to be quite promising due to their larger conjugation and structural diversity that allow remarkable absorption spectra ranging from the UV/Visible to the near-IR region, variable oxidation states that are interconvertible among aromatic, antiaromatic, and nonaromatic compounds, and multi-metal coordinating behaviors. Thereinto, mesohexakis (pentafluorophenyl)-substituted [26] hexaphyrin(1.1.1.1.1.1) which was first synthesized by Cavaleiro [9] in 1999 is an attractive aromatic molecule due to its planar and rectangular shape and strong aromaticity with a 26π conjugated circuit [10–12]. Theoretically, this hexaphyrin (HP) is capable of chelating two metal ions within the macrocycle formed by the two CCNN cores such as doubly N-confused porphyrins (N_2CP) and forming a binuclear coordination complex. However, to the best of our knowledge, only a few metal–HP complexes have been synthesized, for example, the bis-Au_2–HP and mixed bis-AuAg–HP, bis-AuCu–HP complexes, which bear well stabilities, were proposed by Osuka et al. [13,14]. Furthermore, free base HP and its metal complexes exhibit well-resolved and red shifted B- and Q-like absorption bands compared with porphyrins. To better understand the nature of such systems, in this contribution, we present a systematic study of free base HP and its metal complexes using DFT method. The aim of this work is two-fold: (1) to provide detailed descriptions of the ground state electronic structures of these complexes and their precise structural information. In addition, the bonding properties were analyzed by electron localization function (ELF) which is introduced by Becke and Edgecombe [15] and developed by Silvi and co-workers [16,17]. (2) To provide theoretical interpretations of the spectra properties of these complexes. We employed scalar relativistic time-dependent density functional theory (TDDFT) method. Furthermore, the relativistic TDDFT formalism with spin–orbit coupling calculation was also carried out to check the spin–orbit coupling effects on the excitation energies of these complexes. To sum up, we hope this work shed light on the further studies of metal–HP complexes.

2. Computational details

All calculations were carried out with the Amsterdam Density Functional (ADF 2006.01) program package [18–20]. Geometric optimization was calculated using Becke–Perdew (BP) functional with TZP all-electron basis set [21]. Scalar relativistic effects were

* Corresponding authors. Tel.: +86 517 83525379; fax: +86 517 83525369 (Y.-H. Kan).
E-mail addresses: yulanzhu2008@126.com (Y.-L. Zhu), yhkan@yahoo.cn (Y.-H. Kan).

0022-328X/$ - see front matter © 2009 Elsevier B.V. All rights reserved.
doi:10.1016/j.jorganchem.2009.05.002

considered using the zero-order regular approximation (ZORA) [22,23].

TDDFT [24–26] calculations of vertical excitation energies were carried out on the ground state optimized geometries using the asymptotically correct "statistical-average-of-orbital potentials" (SAOP) [27,28] with the TZP basis set. In order to test the solvent effects on the excitation energies of these complexes, the conductor-like continuum solvent model (COSMO) [29–31] was used combined with TDDFT method on the gas phase structures. In addition, we also took into account the effects of spin–orbit coupling on the excitation energies with the relativistic TDDFT formalism which is proposed by Wang and Ziegler [32–34].

To understand the nature of bonding interactions in these metal complexes, we carried out natural bond orbital (NBO) analysis using GENNBO 5.0 program [35]. The bonding properties were also studied according to topological analysis of the ELF, which is defined in terms of the excess of local kinetic energy density due to the Pauli exclusion principle. ELF was calculated with program DGRID 4.0 [36].

3. Results and discussion

3.1. Geometrical structures

The investigated molecules are shown in Fig. 1, containing free base HP, bis-metal and mixed bis-metal complexes. In our calculations, the six pentafluorophenyl in *meso*-carbons were left out. Despite the lack of these groups, the discrepancies of the geometry parameters between the calculated results and experimental data are very small, and this is consistent with the works proposed by Furuta et al. [37]. The key geometry parameters calculated at BP/TZP level are listed in Table 1 together with experimental data of bis-Au_2–HP and mixed bis-AuCu–HP complexes for comparison. Geometry optimization was performed without symmetry constraint. The metalation of HP brings little effects on bond lengths of HP ligand except for dihedral angles. The distortion (for example, dihedral angle N_3–C_4–C_5–N_6 = 20.0°) of free base HP should be ascribed to the steric repulsion between central hydrogens. As shown in Table 1, the agreement between the calculated results and experimental data of bis-Au_2–HP is excellent and the largest deviations for bond lengths and bond angles are 0.12 Å and 2.4°, respectively. Furthermore, all the Au–N bond lengths of the three Au contained complexes range from 2.129 to 2.137 Å. The Au–C bond lengths of these complexes are about 2.03 Å and these data are all slightly smaller than the sum (2.07 Å) of covalent radius of Au and C atoms [38]. The same trends are found for silver and copper series. In addition, it is worth noting that all these complexes exhibit bending shapes. It can be derived from the dihedral angles C_{36}–N_{15}–N_{29}–C_{22} and M_1–N_{15}–N_{29}–M_2 listed in Table 1. From this table, it is obvious that the smallest dihedral angle is found in the bis-Cu_2–HP complex.

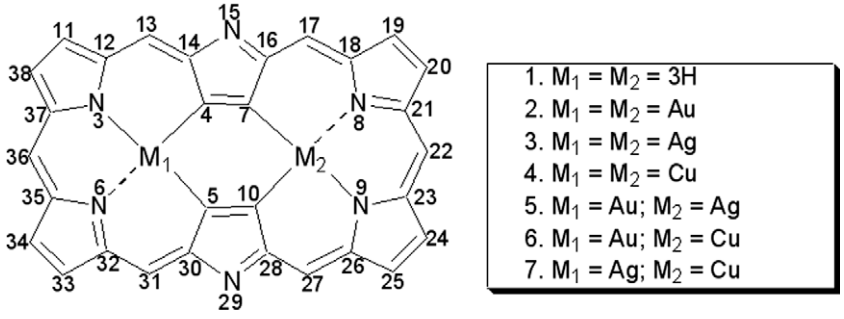

Fig. 1. Hexaphyrin and its group 11 transition metal (III) complexes.

Table 1
Geometry parameters of metal complexes.

Compounds	Au_2HP	Ag_2HP	Cu_2HP	AuAgHP	AuCuHP	AgCuHP
Bond lengths(Å)						
M_1–N_3	2.134(2.105)	2.134	2.002	2.129	2.135(2.051)	2.139
M_1–N_6	2.137(2.113)	2.136	2.004	2.132	2.134(2.014)	2.130
M_1–C_4	2.036(2.037)	2.042	1.929	2.032	2.012(1.940)	2.033
M_1–C_5	2.037(2.024)	2.044	1.930	2.035	2.012(1.941)	2.027
M_2–N_8	2.137(2.101)	2.137	2.002	2.139	2.038(2.038)	2.032
M_2–N_9	2.134(2.099)	2.135	2.003	2.137	2.040(2.042)	2.034
M_2–C_7	2.037(2.018)	2.052	1.930	2.054	1.962(1.983)	1.958
M_2–C_{10}	2.036(2.013)	2.050	1.929	2.053	1.966(2.007)	1.960
M_1–M_2	4.226(4.224)	4.266	4.217	4.251	4.241(4.236)	4.277
Bond angles (°)						
C_{37}–N_3–C_{12}	107.3(106.6)	107.2	105.9	107.4	107.5(106.0)	107.4
C_{35}–N_6–C_{32}	107.2(105.9)	107.2	105.9	107.3	107.5(105.2)	107.5
C_{16}–C_7–C_4	105.3(105.9)	105.7	105.2	105.0	106.3(104.9)	107.0
C_{30}–C_5–C_{10}	105.2(105.1)	105.7	105.3	104.9	106.4(104.0)	107.2
C_{14}–C_4–C_7	105.2(104.5)	105.7	105.3	105.9	104.1(104.3)	103.9
C_{28}–C_{10}–C_5	105.3(104.4)	105.7	105.2	106.0	104.0(106.3)	103.7
C_{18}–N_8–C_{21}	107.2(106.9)	107.4	105.9	107.3	105.3(106.7)	105.3
C_{23}–N_9–C_{26}	107.3(105.5)	107.4	105.9	107.3	105.3(106.1)	105.3
Dihedral angles (°)						
C_{36}–N_{15}–N_{29}–C_{22}	150.4 (153.0)	151.0	136.4	150.7	148.4(141.3)	149.1
M_1–N_{15}–N_{29}–M_2	144.6 (147.3)	146.7	126.6	146.1	141.2(134.5)	143.1

Experimental data are given in parentheses.

Table 2
Natural population analysis (NPA) of these complexes.

	Au_2HP	Ag_2HP	Cu_2HP	AuAgHP	AuCuHP	AgCuHP
M_1	1.356	1.402	1.154	1.361	1.362	1.394
M_2	1.356	1.391	1.154	1.389	1.144	1.149
N_3	−0.5483	−0.5537	−0.5404	−0.5482	−0.5523	−0.5556
N_6	−0.5474	−0.5528	−0.5400	−0.5476	−0.5517	−0.5575
C_4	−0.3499	−0.3603	−0.2730	−0.3624	−0.3417	−0.3318
C_5	−0.3509	−0.3608	−0.2726	−0.3632	−0.3424	−0.3334
C_7	−0.3509	−0.3489	−0.2728	−0.3403	−0.2801	−0.2923
C_{10}	−0.3498	−0.3485	−0.2730	−0.3398	−0.2792	−0.2915
N_8	−0.5475	−0.5519	−0.5404	−0.5524	−0.5331	−0.5338
N_9	−0.5484	−0.5526	−0.5402	−0.5530	−0.5328	−0.5335

3.2. Electronic structures

To explore the electronic structures, NBO and ELF analyses were carried out. Table 2 lists the atomic charges population of these metal complexes from the natural population analysis (NPA) [39] and Fig. 3 displays the ELF density.

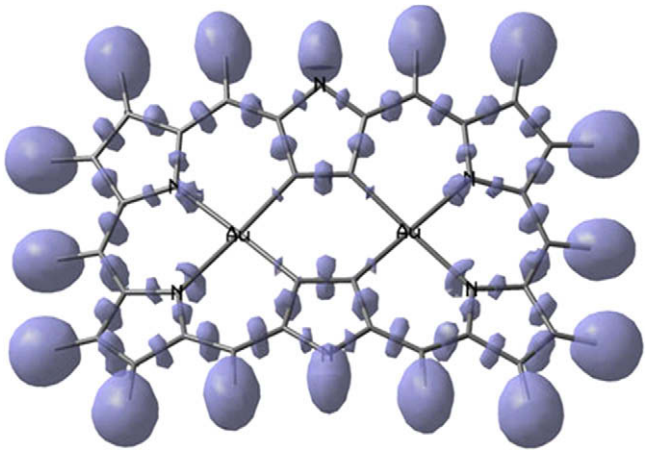

Fig. 2. Three dimensional isosurface with ELF = 0.825.

The NBO related NPA approach can offer us information which is less sensitive to the computational parameters about the interactions between metal atoms and HP ligand [39]. From Table 2, in both bis-M_2–HP and mixed bis-M_2–HP complexes, each kind of metal possesses almost the same positive charge and the "effective" charge is about +1.15 for copper, +1.40 for silver and +1.36 for gold of the neutral molecules, respectively. In particular, the charge of copper is about 0.2 e lower than those of silver and gold atoms. Obviously, they are all quite different from the classical pictures of M_1^{3+} M_2^{3+}– $(HP)^{6-}$. This character is similar to that of metal (Cu^{3+}, Ag^{3+} and Au^{3+}) complexes of *cis*-N_2CP [40]. Since the formed oxidized states of the metals are +3, their lower charges are consistent with slightly covalent interactions between the metal and the nitrogen, carbon atoms of the ligand [39,41]. In order to get more precise information on these metal concerned bonds, bonding situations are thus discussed on the basis of natural localized molecular orbitals (NLMOs) derived from the NBOs. Searching for three-center bond in the NBO was reasonably carried out. From these NBO related analyses, some highlights of these complexes are summarized as follows.

Firstly, the bonding situations of the two same metals in every bis-M_2–HP complexes are the same as each other. Moreover, for Au and Cu species of both bis-M_2–HP and mixed bis-M_2–HP complexes the bonding situations of each kind of metal possess similar bond characters. The higher polarities of the three Au_1–C_4 bonds entirely point to C end, that is, about 58.1%, 58.4% and 54.6% of bis-Au_2–HP, mixed bis-AuAg–HP and mixed bis-AuCu–HP complexes, respectively. The corresponding higher polarities of Au_1–C_5 of the three complexes are 58.2%, 58.5 and 58.3%, respectively. The same trends are found for Cu–C bonds.

Secondly, the lone electron pairs, which are shared by metal atoms, of N atoms in these complexes are also analyzed by NLMO. Taking bis-Au_2–HP as an example, the NLMOs located at N_3, N_6, N_8 and N_9 atoms of bis-Au_2–HP complex are all 84.8%, with "delocalization tails" composed primarily of contributions from Au atoms

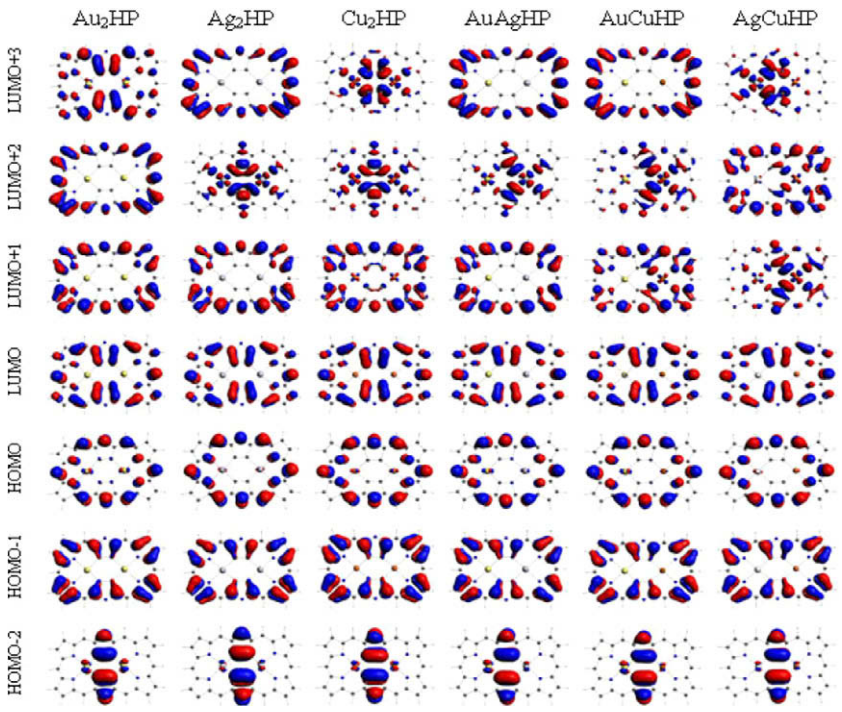

Fig. 3. Frontier molecular orbital pictures of the six complexes.

(7.4% $sd^{2.88}$, 7.3% $sd^{2.92}$, 7.3% $sd^{2.92}$ and 7.4% $sd^{2.88}$, respectively). The other important delocalizations are located at the diagonal core carbons (contributions are all 4.7%). In the mixed bis-AuAg–HP complex, the Au–N bonds have the same NBO properties (localization and delocalization are quantitatively the same) as above. However, in the mixed bis-AuCu–HP, the NLMO located at N_6 is 85.6% with the contributions from Au_1 (5.8% $sd^{1.28}$) and C_4 (4.2%). The NLMO located at N_3 of the complex is 85.5% with the contributions from Au_1 (6.7% $sd^{1.90}$) and C_5 (4.1%). By and large, in all the copper contained complexes, the Cu–N have the same NBO characters, that is, the NLMOs are pretty nearly located at N end (86.2%) with the delocalizations at Cu (6.6% $sd^{1.20}$) and C (3.7%).

Finally, because of the aromaticity of the HP macrocycle [42], three-center bond was analyzed. However, to my surprise, three-center bonds are only found in the bis-Ag_2–HP complex, such as bonds C_5–C_{30}–C_{31}, C_{18}–N_8–C_{21}, C_{27}–C_{28}–N_{29} and C_{22}–C_{23}–N_9. Interestingly, there are also two three-center bonds in which Ag atom participates, namely, bonds C_4–Ag_1–N_6 and C_7–Ag_2–N_8. It is noteworthy that each three-center bond is associated with two three-center antibond NBOs, respectively, which contribute in distinct ways to delocalization interactions.

The ELF analysis yields another point of view on the bonding situation of these complexes. The NBO analysis focuses on MO structures of the molecules, while the ELF analysis considers the total electron-density distribution. The function ELF should demarcate the special regions where there are shared electron interactions as in covalent and metallic bonding and an unshared electron interaction such as ionic bonding. In Fig. 2, the three dimensional representation of spatial areas of localized electrons isosurface (ELF = 0.825) is plotted. We only display the picture of bis-Au_2–HP since the shapes of the other complexes are almost the same. From this picture, we can easily find that there are ELF domains in the C–C, C–N, C–H and N–H bonds of the HP ligand, respectively, and they are consistent with previous reports [43–45]. Furthermore, there are ELF domains between the metal and core atoms, namely, *V*(Au, C) and *V*(Au, N), which indicate the covalent characters for these bonds. The positions of the ELF bonding basins of M–C and M–N bonds are also consistent with their high bond polarities. Especially, these M–N bonding basins surround the corresponding N atoms. Since nitrogen is more electronegative than carbon, the electron density is much more attracted toward the nitrogen than carbon.

3.3. Electronic spectra

The experimental spectra of HP, bis-Au_2–HP and mixed bis-AuAg–HP were measured in CH_2Cl_2. Their gas-phase spectra have not been found by experiment. Thus, solution-phase data are used when the calculated absorption spectra are compared with experimental results. The other four complexes that have not been reported are also computationally investigated for comparison. Table 3 lists the excitation energies, oscillator strengths and main transition configurations computed with TDDFT for the six metal complexes along with experimental data available. In these TDDFT calculations, only singlet-to-singlet transitions were considered. On the other hand, the spin–orbit coupling effects of heavy metal atom should be large. Therefore, the spin-forbidden singlet-to-triplet transitions may appear in the absorption spectra. The relativistic TDDFT calculation with spin–orbit coupling was performed in the next section of this article.

The electronic spectra of bis-Au_2–HP and mixed bis-AuAg–HP complexes were measured in condensed phase [13]. To begin with, we check the effects of solvent on the excitation energies of bis-Au_2–HP complex employing a COSMO correction. However, the solvation has little effect on the excitation energies of bis-Au_2–HP complex. For example, B band of bis-Au_2–HP (1.89 eV) is quite close to the solvent contained theoretical value (1.93 eV) and in good agreement with experimental result (1.84 eV). In the meanwhile, the solvation correction causes a very small blue shift (0.04 eV) of the calculated excitation energy of Q band. Therefore, the following discussions are mainly based on gas phase results.

Because of the important role of frontier molecular orbital (FMO) in the understanding of the electronic spectra of porphyrin derivates, FMO contours and the relative energy levels of FMO

Table 3
Excitation energies (eV), oscillator strengths and main configurations of the spectra of these complexes calculated with TDDFT method along with the experimental data available.

TDDFT/SAOP/TZP			TDDFT/SAOP/TZP		
Excitation	*f*	Main configuration	Excitation	*f*	Main configuration
Au_2HP			*AuAgHP*		
(1.05)			(1.08)		
1.17(1.18)	0.0271	H → L 86.1% H-1 → L+1 12.6%	1.21(1.21)	0.0238	H → L 84.0% H-1 → L+1 14.8%
1.37(1.35)	0.0011	H-1 → L 62.5% H → L+1 36.8%	1.40(1.34)	0.0009	H-1 → L 63.6% H → L+1 35.4%
1.64(1.51)	0.0000	H-2 → L 99.3%	1.73(1.52)	0.0002	H-2 → L 98.9%
1.89(1.85)	0.2030	H → L+1 56.9% H-1 → L 33.4%	1.89(1.85)	0.1511	H → L+1 48.2% H-1 → L 27.0%
1.94(2.00)	0.1394	H-1 → L+1 50.6% H-3 → L 44.3%	1.99(1.90)	0.1737	H-1 → L+1 49.8% H-3 → L 36.3%
Ag_2HP			*AuCuHP*		
1.26	0.0257	H → L 81.3% H-1 → L+1 17.2%	(1.07)		
1.48	0.0003	H-1 → L 59.9% H → L+1 37.6%	1.20(1.20)	0.0212	H → L 83.3% H-1 → L+1 12.7%
1.68	0.0017	H → L+2 95.2%	1.35(1.32)	0.0002	H → L+1 48.2% H → L+2 34.9% H-1 → L 16.5%
1.83	0.0000	H-2 → L 98.5%	1.40	0.0033	H-1 → L 54.5% H → L+2 43.2%
1.91	0.0116	H-1 → L+2 92.2% H-1 → L+1 6.2%	1.59	0.0019	H-1 → L+2 70.4% H-1 → L+1 28.9%
2.05	0.1971	H → L+1 50.5% H-1 → L 30.6%	1.89(1.85)	0.1670	H → L+1 45.4% H-1 → L 25.3% H → L+2 20.0%
2.14	0.1582	H-3 → L 40.9% H-1 → L+1 37.4%	2.05	0.1483	H-3 → L 32.0% H-1 → L+1 30.6% H-1 → L+2 15.9%
Cu_2HP			*AgCuHP*		
1.20	0.0227	H → L 82.5% H-1 → L+1 12.0%	1.24	0.0227	H → L 80.3% H-1 → L+2 12.0%
1.33	0.0006	H → L+1 59.9% H-1 → L 27.4% H → L+2 12.1%	1.26	0.0004	H → L+1 88.2% H → L+2 9.0%
1.40	0.0064	H-1 → L 49.5% H → L+2 46.3%	1.38	0.0021	H-1 → L 69.9% H → L+2 28.6%
1.55	0.0064	H-1 → L+1 49.5% H-1 → L+1 49.2%	1.48	0.0023	H-1 → L+1 83.1% H-1 → L+2 16.1%
1.89	0.1592	H → L+2 38.7% H → L+1 33.5% H-1 → L 19.4%	1.81	0.0002	H-2 → L 98.8%
2.08	0.2603	H-2 → L+1 78.1% H-1 → L+2 6.8%	1.89	0.1624	H → L+2 56.9% H-1 → L 24.6% H → L+1 9.1%
			2.09	0.0527	H-2 → L+1 82.7% H-1 → L+2 7.4%
			2.12	0.2431	H-1 → L+2 40.6% H-4 → L 26.7% H-2 → L+1 15.0%

Experimental data are given in parentheses.

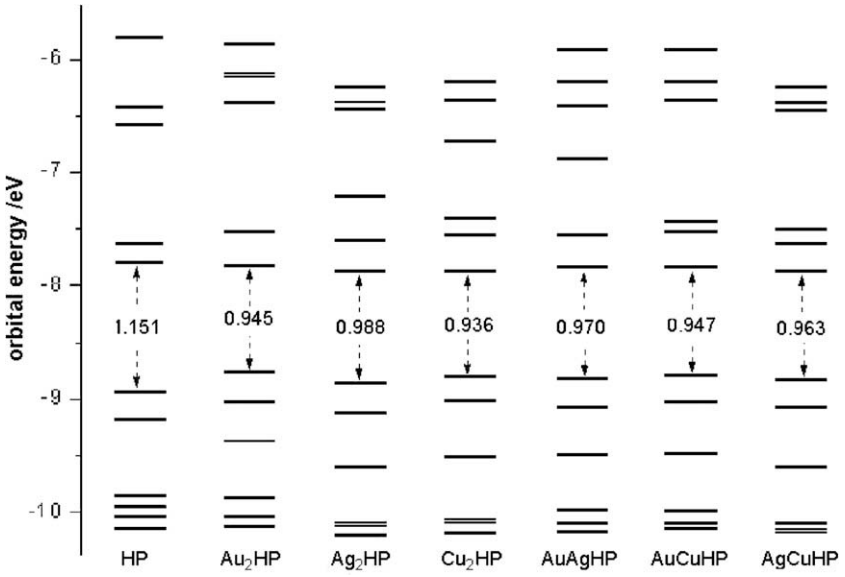

Fig. 4. Molecular orbital energy levels at SAOP/TZP method.

(directly involved in the TDDFT calculation) are shown in Figs. 3 and 4, respectively. Evidently, the HOMO and LUMO of these complexes exhibit the same delocalization and are basically ligand-based orbital. The LUMO+1 of complexes **4**, **6**, **7** and LUMO+2 of complexes **3**, **4**, **5**, **6**, **7** include obvious contributions from metal atoms, particularly, the metal contribution comes mainly from Cu atom for the Cu contained complexes. For complex **2**, the LUMO, LUMO+1, LUMO+2 and HOMOs are all basically ligand-based orbitals. So we can anticipate that the transition natures of the absorption spectra of these complexes will be of different properties. From Fig. 4, we observe that the energy gaps (E_{gap}) of HOMO and LUMO of these complexes exhibit considerably red shift in comparison with those of porphyrins due to the increased π conjugation. E_{gap} of these complexes are in the range of 0.936–0.988 eV. The introduction of transition metals results in smaller E_{gap} of complexes compared with that of free base HP. Interestingly, on the contrary, the metalation of the *cis*-N_2CP leads to larger E_{gap} in the corresponding complexes [39]. The theoretical E_{gap} of these complexes are 0.945, 0.988, 0.936, 0.970, 0.947 and 0.963 eV, respectively, and the corresponding value of free base HP is 1.151 eV. Moreover, as seen in Fig. 4, it is obvious that the destabilizations of HOMOs of these complexes play major roles in the decrease of E_{gap}.

Inspecting the results obtained at TDDFT (SAOP/TZP) method, the following conclusions can be achieved: (1) the absorption spectrum of compound **1** exhibits a strong B-like absorption band at 2.18 eV (568 nm) and rather weak Q-like ones at 1.74 eV (712 nm), 1.38 eV (898 nm), and 1.21 eV (1026 nm) [7,11]. From Table 3, it is clear that both the B- and Q-like bands of the six metal complexes show red shifts compared with those of HP. Furthermore, these complexes possess similar spectra properties, that is, the strong B-like band located at about 1.80–2.15 eV followed by the broad weak Q-like band located at 1.00–1.70 eV. The spectral differences between these complexes are slight. In addition, the absorption spectrum of complex **3** displays its lowest spin-allowed absorption at 1.26 eV which is higher than those of the other metal complexes. (2) The transition nature is different between these seven complexes. For HP, the main contribution is $\pi \rightarrow \pi^*$ transition. However, for these metal complexes, some absorption spectra exhibit LMCT (ligand-to-metal charge transfer) characters due to the contributions from metal atoms of LUMOs. By and large, these six metal complexes can be divided into two groups in terms of transition nature: the first group includes the copper contained complexes **4**, **6**, **7**, and the rest complexes **2**, **3**, and **5** belong to the other group. From Table 3 and Fig. 3, obviously, there is no charge transfer between HP ligand and metal atoms of complexes **2**, and **5**. For complex **3**, only absorption bands 1.68 and 1.91 eV can be assigned to the combination of LMCT and LLCT (ligand-to-ligand charge transfer) transitions due to LUMO+2 involving in the excitations. However, for the copper contained complexes, the transition nature is obviously changed. As seen in Table 3, it is found that almost every absorption band is derived from the combination of LMCT and LLCT transitions. Particularly, in the mixed bis-metal complexes **6** and **7**, it is noteworthy that the copper atom plays a major role in the LMCT process. (3) From Table 3, we can find that there are lowest experimental spectra 1.05 and 1.08 eV for complexes **2** and **3**, respectively, without the corresponding theoretical data. Because in the TDDFT calculations only singlet–singlet transitions were considered, these two lower bands should correspond to the spin-forbidden singlet-to-triplet transitions. Thus, in the next section, the relativistic TDDFT formalism with spin–orbit coupling was carried out to check spin–orbit coupling effects on the absorption spectra of these complexes.

3.4. Spin–orbit coupling effects on excitation energies

In the present ADF version, the relativistic TDDFT formalism which is proposed by Wang and Ziegler [32–34], including spin–orbit coupling is implemented for closed-shell molecules with full use of double-group symmetry. This relativistic TDDFT is based on a two-component and a noncollinear exchange-correlation functional. This TDDFT formalism has the correct nonrelativistic limit and affords the recover three-fold degeneracy of triplet excitations.

Relativistic effect, including scalar relativistic and spin–orbit coupling terms, usually plays an important role in the electronic structures and excited states of systems containing heavy elements. It is necessary to examine the spin–orbit coupling effects on the electronic spectra of complexes **2**–**7** with the above-mentioned relativistic TDDFT formalism. SAOP potential is used with TZP basis set in the relativistic TDDFT calculations. The excitation energies of the relativistic TDDFT calculations for these systems are listed in Table 4 and the scalar relativistic TDDFT results (the

Table 4
The spin–orbit coupling effects on the excitation energies (eV) of these metal complexes.

SAOP		SAOP(spin–orbit)		SAOP		SAOP(spin–orbit)	
Excitation	*f*	Excitation	*f*	Excitation	*f*	Excitation	*f*
Au_2HP				*AuAgHP*			
		0.86	4.3E-7			0.89	1.8E-7
		1.09	6.8E-8			1.11	9.3E-6
		1.14	0.0022			1.16	8.4E-5
1.17	0.0276	1.15	0.0221	1.21	0.0238	1.19	0.0253
1.37	0.0011	1.36	0.0009	1.40	0.0009	1.38	0.0011
		1.44	2.1E-5			1.45	3.0E-6
		1.46	9.6E-7			1.56	1.2E-6
1.64	9.3E-10	1.61	9.9E-7	1.73	0.0002	1.71	3.6E-4
		1.78	2.3E-5			1.86	0.0140
1.89	0.2030	1.88	0.1881	1.89	0.1511	1.89	0.1436
1.94	0.1394	1.92	0.1210			1.92	2.9E-4
		1.96	0.0028	1.99	0.1737	1.97	0.1553
Ag_2HP				*AuCuHP*			
		0.90	2.5E-8			0.86	1.0E-7
		1.12	2.9E-7			1.09	2.2E-5
		1.17	5.1E-6			1.16	6.0E-5
1.26	0.0257	1.23	0.0263	1.20	0.0212	1.18	0.0271
1.48	0.0003	1.39	0.0012			1.33	1.2E-5
		1.45	9.9E-7	1.35	0.0002	1.33	0.0010
		1.64	6.5E-7	1.40	0.0033	1.38	0.0028
		1.65	4.0E-7			1.44	6.3E-6
1.68	0.0017	1.67	0.0049			1.54	5.4E-7
1.83	2.5E-5	1.81	1.5E-5			1.58	2.1E-5
		1.90	0.0034	1.59	0.0019	1.59	0.0026
		1.90	0.0346			1.87	0.0316
1.91	0.0116	1.92	0.1732	1.89	0.1670	1.89	0.1358
		1.94	0.0002	2.05	0.1483	2.00	0.1871
2.05	0.1971	2.06	0.2300				
2.14	0.1582	2.12	0.0002				
Cu_2HP				*AgCuHP*			
		0.85	6.3E-9			0.88	1.3E-8
		1.06	1.3E-7			1.10	2.6E-7
		1.16	3.2E-5			1.15	1.4E-5
1.20	0.0227	1.18	0.0278	1.24	0.0227	1.21	0.0284
1.33	0.0006	1.31	0.0021			1.24	1.5E-7
		1.35	2.4E-6	1.26	0.0004	1.25	5.8E-5
1.40	0.0064	1.38	0.0051	1.38	0.0021	1.37	0.0037
		1.42	6.3E-7			1.42	3.6E-7
		1.55	1.4E-5	1.48	0.0023	1.48	0.0022
1.55	0.0064	1.55	0.0068			1.50	3.0E-7
		1.58	9.7E-9			1.64	8.2E-8
1.74	1.6E-5	1.72	7.9E-7	1.81	0.0002	1.81	2.2E-4
		1.88	0.0055	1.89	0.1624	1.89	0.1245
1.89	0.1592	1.88	0.1456			1.90	0.0408
		2.02	3.2E-5			2.02	1.7E-5
		2.06	0.0049	2.09	0.0527	2.07	0.1861
2.08	0.2603	2.08	0.3093	2.12	0.2431	2.08	0.1126

same as in Table 3) are synchronously listed to demonstrate the effects of spin–orbit coupling on the excitation energies. Firstly, from Table 4, we detect that spin–orbit coupling has almost no effect on the singlet excited states and the average difference in energy is mere 0.017 eV. In other words, whether spin–orbit coupling is included, the main feature of the theoretical spectra is about the same in terms of excitation energies. In the relativistic TDDFT results, the spin-forbidden singlet-to-triplet transition appears as weak tails in the absorption spectra of these complexes and they are all systematically three-fold degeneracy, furthermore, it is noteworthy that all their oscillator strengths are very small. Theoretically, when spin–orbit coupling is included, it should substantially mix singlet and triplet excited states. However, for these metal complexes, the degree of mixes of singlet and triplet excited states is very low. For example, the band 1.15 eV of complex **2** with oscillator strength 0.0221 mainly consists of singlet excited state (91%). The band 1.92 eV of complex **3** is mainly composed of three singlet excited states and one triplet excited state, but the major composition is also the singlet excited state (99%). For complex **4**, band 1.38 and 1.55 eV are both pure singlet excited states. The ratio of singlet excited states of band 1.88 and 2.08 eV are 96.2% and 98.4%, respectively. For mixed bis-M_2–HP complexes, the three singlet excited states 1.89 eV and triplet excited states 1.86, 1.87 and 1.90 eV of AuAgHP, AuCuHP and AgCuHP are mixed states of singlet and triplet excited states. However, the percentages of the dominative states are all larger than 75%. In conclusion, the effects of spin–orbit coupling on the electronic spectra of complexes **2**–**7** are small that it is safe enough to neglect spin–orbit coupling effects for these systems.

4. Conclusions

In this work, DFT is applied to study the properties of HP and its group 11 transition metal complexes. The electronic structures and geometrical parameters of these molecules have been investigated and compared. In addition, the bonding situations of these complexes are analyzed with NBO approach and ELF topological analysis. From the NBO related NPA and NLMO analyses, it is concluded

that M–C and M–N bonds are all polarized toward C and N atoms and show slightly covalent characters. The covalent properties are also proved by ELF due to the ELF basins of these bonds. The excitation energies of HP and its group 11 transition metal complexes have been computed with the scalar-ZORA TDDFT. The metalation leads to red shifts in the spectra of these complexes with respect to free base HP. We have also calculated electronic spectra of these metal complexes using the relativistic TDDFT with spin–orbit coupling included. However, the effects of spin–orbit coupling on the electronic spectra of complexes are so small that it is safe enough to neglect spin–orbit coupling for these systems.

Acknowledgments

We acknowledge support from the National Natural Science Foundation of China (Nos. 20703008 and 20671038), Program for Changjiang Scholars and Innovative Research Team in University (IRT0714), the Natural Science Foundation of Jiangsu Educational Office (No. 06KJD150031) and the Opening Project of Key Laboratory for Chemistry of Low-Dimensional Materials of Jiangsu Province (No. JSKC06032).

References

[1] A. Jasat, D. Dolphin, Chem. Rev. 97 (1997) 2267.
[2] J.Y. Shin, H. Furuta, K. Yoza, S. Igarashi, A. Osuka, J. Am. Chem. Soc. 123 (2001) 7190.
[3] A. Srinivasan, T. Ishizuka, A. Osuka, H. Furuta, J. Am. Chem. Soc. 125 (2003) 878.
[4] M. Suzuki, M.C. Yoon, D.Y. Kim, J.H. Kwon, H. Furuta, D. Kim, A. Osuka, Chem. Eur. J. 12 (2006) 1754.
[5] J.L. Sessler, D. Seidel, Angew. Chem., Int. Ed. 42 (2003) 5134.
[6] S. Shimizu, R. Taniguchi, A. Osuka, Angew. Chem., Int. Ed. 44 (2005) 2225.
[7] M. Suzuki, R. Taniguchi, A. Osuka, Chem. Commun. (2004) 2682.
[8] J.H. Kwon, T.K. Ahn, M.C. Yoon, D.Y. Kim, M.K. Koh, D. Kim, H. Furuta, M. Suzuki, A. Osuka, J. Phys. Chem. B 110 (2006) 11683.
[9] M.G.P.M.S. Neves, R.M. Martins, A.C. Tomé, A.J.D. Silvestre, A.M.S. Silva, V. Félix, M.G.B. Drew, J.A.S. Cavaleiro, Chem. Commun. (1999) 385.
[10] X.J. Zhu, S.T. Fu, W.K. Wong, J.P. Guo, W.Y. Wong, Angew. Chem., Int. Ed. 45 (2006) 3150.
[11] T.K. Ahn, J.H. Kwon, D.Y. Kim, D.W. Cho, D.H. Jeong, S.K. Kim, M. Suzuki, S. Shimizu, A. Osuka, D. Kim, J. Am. Chem. Soc. 127 (2005) 12856.
[12] K. Youfu, A. Osuka, Org. Lett. 7 (2005) 4381.
[13] S. Mori, A. Osuka, J. Am. Chem. Soc. 127 (2005) 8030.
[14] S. Mori, A. Osuka, Inorg. Chem. 47 (2008) 3937.
[15] A. Becke, K. Edgecombe, J. Chem. Phys. 92 (1990) 5397.
[16] B. Silvi, A. Savin, Nature 371 (1994) 683.
[17] A. Savin, A. Becke, D. Flad, R. Nesper, H. Preuss, Angew. Chem., Int. Ed. 30 (1991) 409.
[18] G.T. Velde, F.M. Bickelhaupt, E.J. Baerends, C.F. Guerra, S.J.A.V. Gisbergen, J.G. Snijders, T. Ziegler, J. Comput. Chem. 22 (2001) 931.
[19] C.F. Guerra, J.G. Snijders, G.T. Velde, E.J. Baerends, Theor. Chem. Acc. 99 (1998) 391.
[20] G.T. Velde, E.J. Baerends, J. Comput. Phys. 99 (1992) 84.
[21] J.P. Perdew, Phys. Rev. B 33 (1986) 8822.
[22] E. Vanlenthe, E.J. Baerends, J.G. Snijders, J. Chem. Phys. 99 (1993) 4597.
[23] E. Vanlenthe, E.J. Baerends, J.G. Snijders, J. Chem. Phys. 101 (1994) 9783.
[24] S.J.A.V. Gisbergen, F. Kootstra, P.R.T. Schipper, O.V. Gritsenko, J.G. Snijders, E.J. Baerends, Phys. Rev. A 57 (1998) 2556.
[25] C. Jamorski, M.E. Casida, D.R. Salahub, J. Chem. Phys. 104 (1996) 5134.
[26] R. Bauernschmitt, R. Ahlrichs, Chem. Phys. Lett. 256 (1996) 454.
[27] P.R.T. Schipper, O.V. Gritsenko, S.J.A. van Gisbergen, E.J. Baerends, J. Chem. Phys. 112 (2000) 1344.
[28] A. Rosa, G. Ricciardi, E.J. Baerends, S.J.A. van Gisbergen, J. Phys. Chem. A 105 (2001) 3311.
[29] A. Klamt, G. Schürmann, J. Chem. Soc., Perkin Trans. 2 (1993) 799.
[30] A. Klamt, J. Phys. Chem. 99 (1995) 2224.
[31] A. Klamt, V. Jonas, J. Chem. Phys. 105 (1996) 9972.
[32] F. Wang, T. Ziegler, J. Chem. Phys. 122 (2005) 204103.
[33] F. Wang, T. Ziegler, J. Chem. Phys. 123 (2005) 194102.
[34] F. Wang, T. Ziegler, J. Chem. Phys. 123 (2005) 154102.
[35] E.D. Glendening, J.K. Badenhoop, A.E. Reed, J.E. Carpenter, J.A. Bohmann, C.M. Morales, F. Weinhold, NBO 5.0 Theoretical Chemistry Institute, University of Wisconsin, Madison, WI, 2001.
[36] M. Kohout, Program DGRID, version 4.0, Max-Planck Institut für Chemische Physik fester Stoffe, Dresden, 2006.
[37] H. Furuta, H. Maeda, A. Osuka, J. Org. Chem. 65 (2000) 4222.
[38] L. Pauling, The Nature of the Chemical Bond and the Structure of Molecules and Crystals. An Introduction to Modern Structural Chemistry, Cornell University Press, Ithaca, NY, H. Milford, Oxford University Press, London, 1939.
[39] A.E. Reed, L.A. Curtiss, F. Weinhold, Chem. Rev. 88 (1988) 899.
[40] Y.L. Zhu, S.Y. Zhou, Y.H. Kan, L.K. Yan, Z.M. Su, J. Chem. Phys. 126 (2007) 245106.
[41] L. Petit, C. Adamo, N. Russo, J. Phys. Chem. B 109 (2005) 12214.
[42] J. Sankar, S. Mori, S. Saito, H. Rath, M. Suzuki, Y. Inokuma, H. Shinokubo, K.S. Kim, Z.S. Yoon, J.-Y. Shin, J.M. Lim, Y. Matsuzaki, O. Matsushita, A. Muranaka, N. Kobayashi, D. Kim, A. Osuka, J. Am. Chem. Soc. 130 (2008) 13568.
[43] P. Soler, F. Fuster, H. Chevreau, J. Comput. Chem. 25 (2004) 1920.
[44] S. Berski, B. Silvi, Z. Latajka, J.L. Eszczyński, J. Chem. Phys. 111 (1999) 2542.
[45] A. Scemama, P. Chaquin, M. Caffarel, J. Chem. Phys. 121 (2004) 1724.